Ocean Sci. Discuss., 10, 473–517, 2013
www.ocean-sci-discuss.net/10/473/2013/
doi:10.5194/osd-10-473-2013

Ocean Science
Discussions
Open Access

A practical scheme to introduce explicit tidal forcing into OGCM

K. Sakamoto, H. Tsujino, H. Nakano, M. Hirabara, and G. Yamanaka

Oceanographic Research Department, Meteorological Research Institute, Nagamine, Tsukuba, Ibaraki 305-0052, Japan

Received: 14 February 2013 – Accepted: 20 February 2013 – Published: 7 March 2013

Correspondence to: K. Sakamoto (ksakamot@mri-jma.go.jp)

Published by Copernicus Publications on behalf of the European Geosciences Union.

A practical scheme to introduce explicit tidal forcing into OGCM

K. Sakamoto et al.

Abstract

A practical scheme is proposed to introduce tides explicitly into ocean general circulation models (OGCM). In this scheme, barotropic linear response to the tidal forcing is calculated by the time differential equations modified for ocean tides, instead of the original barotropic equations of OGCM. This allows usage of various parameterizations specified for tides, such as the self attraction/loading (SAL) effect and energy dissipation due to internal tides, without unintentional violation of the original dynamical balances in OGCM. Meanwhile, secondary nonlinear effects of tides, e.g. excitation of internal tides and advection by tidal currents, are fully represented in the framework of the original OGCM equations. That is, this scheme drives OGCM by the barotropic linear tidal currents which are predicted progressively by a well-tuned tide model, instead of the equilibrium tide potential, without large additional numerical costs. We incorporated this scheme into Meteorological Research Institute Community Ocean Model and executed test experiments with a low-resolution global model. The results showed that the model can simulate both of non-tidal circulations and tidal motion simultaneously. Owing to usage of tidal parameterizations such as a SAL term, a root mean square error in the tidal heights was as small as 10.0 cm, which is comparable to tide models tuned elaborately. In addition, analysis of speed and energy of the barotropic tidal currents was consistent with past tide studies. The model also showed active excitement of internal tides and tidal mixing. Their impacts should be examined using a model with a finer resolution in future, since explicit and precise introduction of tides into OGCM is a significant step toward upgrade of ocean modeling.

1 Introduction

Recent advances in theories of ocean general circulations and observations of deep seas have revealed that tides play a significant role in open oceans, as well as in coastal areas. As a representative study, Munk and Wunsch (1998) suggested that

OSD
10, 473–517, 2013

vertical mixing in deep seas due to breaking of internal tides is an important process in the global thermohaline circulations. This hypothesis is supported by the fact that a large part of the tidal energy is dissipated in deep seas (St. Laurent and Garrett, 2002; Egbert and Ray, 2001; Niwa and Hibiya, 2011). In addition, various studies reported that local strong tidal mixing affects ocean circulations with a basin scale. For example, tidal mixing near the Kuril Islands plays an important role in the formation process of the water mass called North Pacific Intermediate Water (Nakamura and Awaji, 2004; Osafune and Yasuda, 2006). Tidal mixing in the Arctic shelf seas modifies the salinity budget through interaction with sea ice, and, as a result, the deep thermohaline circulation in the North Atlantic (Postlethwaite et al., 2011). In a similar fashion, tidal mixing over the Antarctic shelves affects the formation process of Antarctic Bottom Water (Pereira et al., 2002; Robertson, 2001a,b). These studies commonly indicate importance of tides in general circulations.

Meanwhile, tidal processes were not sufficiently taken into account in traditional ocean general circulation models (OGCM) for a long period. One reason is that most of them could not represent tides since they adopted the rigid-lid condition to preclude the surface gravity waves due to the CFL condition. Another is that tidal motions with a time scale of half or one day were omitted intentionally to focus on variations with longer time scales in geostrophic currents. Recently, effects of tides have begun to be considered in OGCM, stimulated by advances in the studies of tides.

The methodology to incorporate tides into OGCM is classified into the two types, i.e. the implicit one and the explicit one. The implicit type uses indirect parameterizations about tidal effects rather than simulating tides themselves, to avoid drastic change of the OGCM framework. A typical parameterization adopted by various recent OGCMs is mixing enhancement in deep seas and coastal areas (e.g. St. Laurent and Garrett, 2002). Lee et al. (2006) reported that this kind of parameterization contributes to good representation of the salinity distribution in the North Atlantic. As another indirect parameterization, Bessiéres et al. (2008) proposed a way to parameterize the tidal residual currents in OGCM.

OSD
10, 473–517, 2013

The explicit type introduces the tidal dynamics into free-surface OGCM directly. Though this type needs large computer resources and modification of a part of the OGCM framework, some achievements have been already reported. For example, Schiller and Fiedler (2007) improved model representation of water transport and mixing in the Indonesian Through Flow region and Autstralian shelves. Müller et al. (2010) reported improvement in modeling of the pathway of the North Atlantic Current and water-modification processes in the North Atlantic. In addition, Arbic et al. (2010) discussed a possibility that explicit incorporation of tides into an eddy-resolving OGCM may lead to drastic improvement in representation of various ocean processes, such as interaction between meso-scale eddies and tides, form drag on the sea mounts, excitement and propagation of internal tides in realistic three-dimensional stratification, and so on. Development of OGCM which simulates simultaneously time evolution of the tidal field and the non-tidal field (called the basic field hereafter), is now a frontier in ocean modeling.

On the other hand, modeling of tides themselves has been developed virtually independently of OGCM, based on barotropic ocean models. Many modeling studies have shown that dynamics particular to tides need to be introduced into the model equations for accurate representation of tides (e.g. Matsumoto et al., 2000). A typical example is the self attraction/loading (SAL) effect. This represents modification of the gravity field and elastic deformation of the bottom ground induced by movement of ocean water (Schwiderski, 1980). Due to the SAL effect, the pressure gradient term accompanied by the tidal height gradient $\nabla\eta$ is modified in the equation of barotropic motion as follows

$$-g\nabla\eta \Rightarrow -g\nabla(\eta-\eta_{\mathrm{SAL}}). \tag{1}$$

In order to represent the gravity change of the self attraction and the loading effect, which is that the sea surface elevation induced by convergence of barotropic currents is cancelled partly by depression of the bottom ground due to water weight, the elevation is subtracted by η_{SAL} in calculation of the pressure gradient. Though various

OSD
10, 473–517, 2013

A practical scheme to introduce explicit tidal forcing into OGCM

K. Sakamoto et al.

evaluations of η_{SAL} have been proposed, a linear response is used as a first-order approximation

$$\eta_{SAL} = (1-\alpha)\eta, \tag{2}$$

where α is a constant between 0.88 and 0.95 (Matsumoto et al., 2000). Under this approximation of SAL, the pressure gradient term $-g\nabla\eta$ is modified into $-g\alpha\nabla\eta$.

Another issue of tide modeling is energy dissipation of tides, such as energy transfer to internal tides and form drag by bottom topography on tidal currents. In general, as model resolution becomes finer, model can represent more kinds of dissipation processes without parameterization. However, considering that internal tide processes can not be reproduced sufficiently even in a model with a horizontal resolution of 10 km, which is considerably fine at present (Niwa and Hibiya, 2011), a parameterization specialized for dissipation is still necessary to represent tides with good accuracy (Jayne and St. Laurent, 2001; Arbic et al., 2004). Furthermore, various parameterizations unusual for OGCM have been proposed for tide modeling, such as body tide and atmospheric tide. See Chapt. 6 of Kantha and Clayson (2000) for detail.

The knowledge which has been obtained by tide modeling studies should be exploited in order to introduce tides into OGCM with high accuracy. However, this is a difficult task, since dynamical balances in the basic field of OGCM are violated if terms proposed for tide modeling are incorporated into the OGCM equations directly (Arbic et al., 2010). For example, the SAL term of Eq. (1) changes the geostrophic relationship between sea surface gradient and currents. Parameterizations for dissipation of tidal currents are not suited for the geostrophic currents in OGCM, either, since their time scales of change are so different that their dissipation mechanisms are not same. Therefore, we cannot replace simply the governing equations of OGCM by those of tide modeling. The two sets of the governing equations should be harmonized by some means in introducing tides into OGCM.

This problem has not been solved yet. In most of the model studies introducing tides explicitly into OGCM, the equilibrium tide potential is given directly to the free-surface

OSD
10, 473–517, 2013

barotropic equation of motion, and the tidal and basic fields are calculated without separation (Thomas et al., 2001; Schiller, 2004; Schiller and Fiedler, 2007; Müller et al., 2010). In these studies, the problem due to the differences between the tidal and basic (geostrophic) characteristics is not investigated sufficiently. To the best of our knowledge, Arbic et al. (2010), who introduced tides into an eddy-resolving global OGCM, examined this problem most carefully. Though they calculated time evolution of the tidal and basic fields without separation as in other studies, they elaborated a method to prevent the parameterizations specialized for tides from affecting the basic fields. Specifically, they defined the tidal currents as velocity deviation from 25-h running mean, which is calculated progressively in the model, and restricted the tidal dissipation parameterization to work on the tidal currents only. In addition, they defined the tidal height as sea surface height (SSH) deviation from the dynamical height, which is calculated every time step, and evaluated the SAL term only for it in order that SAL should not contaminate the basic field (e.g. geostrophic currents). However, their method is expected to expend a substantial amount of numerical resources. Furthermore, it seems questionable that all of the SSH deviation is treated as the tidal height.

As a solution of the problem, we propose a new practical scheme to incorporate tides explicitly into OGCM. This scheme is based on the recognition that the governing equations are different between the tidal and basic fields, and calculates their time evolutions separately. This approach is in contrast to traditional typical schemes such as Schiller (2004) where the tidal and basic fields are given by the basically same governing equations.

First, this paper will explain the scheme in detail. Next, model representations of tides by this scheme will be shown based on some test experiments of a global OGCM. Finally, tidal effects on the basic fields in the OGCM will be presented briefly though they are preliminary results.

OSD
10, 473–517, 2013

2 Scheme and model

2.1 Conventional scheme

Before presenting the new tide scheme, we show the scheme of Schiller (2004) as a representative example of the traditional schemes where the tidal forcing is incorporated directly into the governing equations. First, the original standard expressions of the barotropic equations of motion and continuity are

$$\frac{\partial \boldsymbol{U}}{\partial t} + f\boldsymbol{k}\times\boldsymbol{U} = -g(\eta+H)\nabla\eta + \boldsymbol{D} + \boldsymbol{\tau}^{\mathrm{btm}} + \boldsymbol{X} \tag{3}$$

$$\frac{\partial \eta}{\partial t} + \nabla\cdot\boldsymbol{U} = F_{\mathrm{w}}, \tag{4}$$

where $\boldsymbol{U}$ is the vertically integrated transport vector, η the SSH anomaly, f the Coriolis parameter, $\boldsymbol{k}$ the upward vertical unit vector, g the gravitational acceleration, H the water depth, $\boldsymbol{D}$ a dissipation parameterization, τ^{btm} the bottom friction (already divided by standard density), $\boldsymbol{X}$ the other residual terms including the vertically integrated advection and the wind stress, and F_{w} is the surface water flux. Introducing of tides means that the equilibrium tide potential η_0 and the SAL term η_{SAL} are added, and $\boldsymbol{D}$ is changed to the dissipation parameterization specialized for tides, which is indicated by $\boldsymbol{D}_{\mathrm{modified}}$, as

$$\frac{\partial \boldsymbol{U}}{\partial t} + f\boldsymbol{k}\times\boldsymbol{U} = -g(\eta+H)\nabla(\eta-\beta\eta_0-\eta_{\mathrm{SAL}}) + \boldsymbol{D}_{\mathrm{modified}} + \boldsymbol{\tau}^{\mathrm{btm}} + \boldsymbol{X}, \tag{5}$$

where β represents the body tide effect (Schwiderski, 1980). If the linear approximation for the SAL term, Eq. (2), is adopted, Eq. (5) becomes

$$\frac{\partial \boldsymbol{U}}{\partial t} + f\boldsymbol{k}\times\boldsymbol{U} = -g(\eta+H)\nabla(\alpha\eta-\beta\eta_0) + \boldsymbol{D}_{\mathrm{modified}} + \boldsymbol{\tau}^{\mathrm{btm}} + \boldsymbol{X}. \tag{6}$$

OSD
10, 473–517, 2013

A practical scheme to introduce explicit tidal forcing into OGCM

K. Sakamoto et al.

This is equivalent to a standard barotropic tide model, e.g. the continuous ocean tide equations of Schwiderski (1980). In this traditional scheme, the time evolutions of $\boldsymbol{U}$ and η under the tidal forcing are obtained by solving Eqs. (4) and (5) (or Eq. 6) under $\eta_0(x,y,t)$, which is analytically calculated.

This scheme works well in modeling tides only, however, in modeling of the tidal and basic fields simultaneously, it induces the problem that the terms specialized for tides affect the basic fields unintentionally. Actually, Eq. (6) shows clearly that the SAL term changes the relationship between the sea surface gradient and the barotropic currents. The dissipation $\boldsymbol{D}_{\mathrm{modified}}$ also changes the basic currents. Introduction of parameterizations specified for tides results in violation of the dynamical balances in the basic fields.

2.2 New scheme

The cause of the problem is that the barotropic equation of motion for tides Eq. (5) is different from the OGCM standard equation for the basic fields Eq. (3). Therefore, the new tide scheme calculates the tidal and basic fields by the two different equations as explained below. The focus of the scheme is to achieve simultaneously both of accurate modeling of tides and maintenance of the dynamical balances in the original OGCM.

The basis of the scheme is decomposition of the variables, $\boldsymbol{U}$, η, $\boldsymbol{D}$ and $\boldsymbol{\tau}^{\mathrm{btm}}$ in the barotropic equations into the linear tidal component and the basic component,

$$\boldsymbol{U} = \boldsymbol{U}_{\mathrm{b}} + \boldsymbol{U}_{\mathrm{lt}} \tag{7}$$

$$\eta = \eta_{\mathrm{b}} + \eta_{\mathrm{lt}} \tag{8}$$

$$\boldsymbol{D} = \boldsymbol{D}_{\mathrm{b}} + \boldsymbol{D}_{\mathrm{lt}} \tag{9}$$

$$\boldsymbol{\tau}^{\mathrm{btm}} = \boldsymbol{\tau}_{\mathrm{b}}^{\mathrm{btm}} + \boldsymbol{\tau}_{\mathrm{lt}}^{\mathrm{btm}}. \tag{10}$$

The linear tidal component indicated by the subscript lt corresponds to the primary response of the barotropic ocean to the equilibrium tide potential. The basic component with the subscript b is the other barotropic and baroclinic motions, including all of the

OSD
10, 473–517, 2013

dynamical processes in the original OGCM and the secondary effects of tides (e.g. internal tides, tidal advection, bottom shear of tidal currents and so on).

Each of the two components is calculated by its own governing equation. The linear tidal component is governed by the equations for tide modeling, i.e. Eq. (5) and the equation of continuity except for $\boldsymbol{X}$,

$$\frac{\partial \boldsymbol{U}_{\mathrm{lt}}}{\partial t} + f\boldsymbol{k} \times \boldsymbol{U}_{\mathrm{lt}} = -g(\eta + H)\nabla(\eta_{\mathrm{lt}} - \beta\eta_0 - \eta_{\mathrm{SAL}}) + \boldsymbol{D}_{\mathrm{lt}} + \boldsymbol{\tau}_{\mathrm{lt}}^{\mathrm{btm}} \tag{11}$$

$$\frac{\partial \eta_{\mathrm{lt}}}{\partial t} + \nabla \cdot \boldsymbol{U}_{\mathrm{lt}} = 0. \tag{12}$$

The basic component is governed by the standard OGCM equations, i.e. Eqs. (3) and (4)

$$\frac{\partial \boldsymbol{U}_{\mathrm{b}}}{\partial t} + f\boldsymbol{k} \times \boldsymbol{U}_{\mathrm{b}} = -g(\eta + H)\nabla\eta_{\mathrm{b}} + \boldsymbol{D}_{\mathrm{b}} + \boldsymbol{\tau}_{\mathrm{b}}^{\mathrm{btm}} + \boldsymbol{X} \tag{13}$$

$$\frac{\partial \eta_{\mathrm{b}}}{\partial t} + \nabla \cdot \boldsymbol{U}_{\mathrm{b}} = F_{\mathrm{w}}. \tag{14}$$

The numerical procedure to predict the two components by the above equations is schematically illustrated by Fig. 1. Generally in a free-surface OGCM, starting from velocity $\boldsymbol{u}$ and SSH η at the time step N, those at the next step $N+1$ are calculated using the equations of motion and continuity, and usually the barotropic and baroclinic constituents are predicted differently in the calculation (so called mode splitting, indicated by $\hat{\boldsymbol{u}}$, $\boldsymbol{U}$ and η in Fig. 1). The key of the new scheme is to split the barotropic constituent into the basic and linear tidal components, further ($\boldsymbol{U}_{\mathrm{b}}, \eta_{\mathrm{b}}, \boldsymbol{U}_{\mathrm{lt}}$ and η_{lt}), and to calculate time evolution of $\boldsymbol{U}_{\mathrm{lt}}$ and η_{lt} almost independently. The solid arrow related to $\boldsymbol{U}_{\mathrm{lt}}$ and η_{lt} in Fig. 1 indicates this independent calculation, while the dashed arrow means that $\boldsymbol{U}_{\mathrm{b}}$ and η_{b} are given by subtraction, i.e. $\boldsymbol{U} - \boldsymbol{U}_{\mathrm{lt}}$ and $\eta - \eta_{\mathrm{lt}}$, respectively. That is, the three sets of the governing equations are calculated at each time step, and the three-dimensional velocity field at the next step is made by summation of them.

OSD
10, 473–517, 2013

A practical scheme to introduce explicit tidal forcing into OGCM

K. Sakamoto et al.

The linear terms in the barotropic equations, such as the Coriolis force and the Laplacian horizontal viscosity, can be split into the basic and linear tidal components naturally, while the non-linear terms should be treated carefully. In the scheme, all of the advection terms are incorporated into the basic equations ($\boldsymbol{X}$ in Eq. 13), and the linear tidal equations have no advection. Specifically, the tracer and momentum advections are calculated using the three dimensional velocity field given by summation of all the components ($\boldsymbol{u}$ in Fig. 1), and they are added to the basic equations. This is based on the assumption of the scheme: the linear tidal component represents only the linear primary response to the tidal forcing, and the other secondary effects, such as tidal advection and internal tides, are represented by the basic component. Modification of the tides due to interaction between tidal currents and basic fields is also represented by the basic equations as secondary oscillations with tidal frequencies (see Appendix A for detail).

The bottom friction $\boldsymbol{\tau}^{\text{btm}}$ is also non-linear, when expressed by a quadratic form as (Weatherly et al., 1980)

$$\boldsymbol{\tau}^{\text{btm}} = -C_{\text{D}} \left| \frac{\boldsymbol{U}}{H+\eta} \right| \mathbf{T}_{\theta} \frac{\boldsymbol{U}}{H+\eta}. \tag{15}$$

The constant C_{D} indicates a drag coefficient and $\mathbf{T}_{\theta}$ a matrix representing horizontal veering,

$$\mathbf{T}_{\theta} = \begin{pmatrix} \cos\theta & -\sin\theta \\ \sin\theta & \cos\theta \end{pmatrix}, \tag{16}$$

where θ is the veer angle. There are various ways to split Eq. (15) into the term for the basic barotropic equation and that for the linear tidal equation. For simplicity of the equations, we decided that a sum of the two components is used for $|\boldsymbol{U}/(H+\eta)|$ (the

OSD
10, 473–517, 2013

coefficient part) while each component for $\boldsymbol{U}/(H+\eta)$ (the vector part),

$$\boldsymbol{\tau}_{\mathrm{b}}^{\mathrm{btm}} = -C_{\mathrm{D}} \left| \frac{\boldsymbol{U}_{\mathrm{b}} + \boldsymbol{U}_{\mathrm{lt}}}{H+\eta} \right| \mathbf{T}_{\theta} \frac{\boldsymbol{U}_{\mathrm{b}}}{H+\eta} \tag{17}$$

$$\boldsymbol{\tau}_{\mathrm{lt}}^{\mathrm{btm}} = -C_{\mathrm{D}} \left| \frac{\boldsymbol{U}_{\mathrm{b}} + \boldsymbol{U}_{\mathrm{lt}}}{H+\eta} \right| \mathbf{T}_{\theta} \frac{\boldsymbol{U}_{\mathrm{lt}}}{H+\eta}. \tag{18}$$

Using the new scheme, we can avoid the violation of the dynamical balance in the basic field. To show this achievement clearly, we assume the SAL term in a linear form as $\eta_{\mathrm{SAL}} \sim (1-\alpha)\eta_{\mathrm{lt}}$ and sum Eqs. (13) and (11),

$$\frac{\partial \boldsymbol{U}}{\partial t} + f\boldsymbol{k} \times \boldsymbol{U} = -g(\eta + H)\nabla(\eta_{\mathrm{b}} + \alpha\eta_{\mathrm{lt}} - \beta\eta_0) + \boldsymbol{D}_{\mathrm{b}} + \boldsymbol{D}_{\mathrm{lt}} + \boldsymbol{\tau}_{\mathrm{b}}^{\mathrm{btm}} + \boldsymbol{\tau}_{\mathrm{lt}}^{\mathrm{btm}} + \boldsymbol{X}. \tag{19}$$

This equation of motion clearly changes from the conventional scheme, Eq. (6). The SAL effect (α) works for η_{lt} only, and the expressions for dissipation and bottom friction for tides ($\boldsymbol{D}_{\mathrm{lt}}$ and $\boldsymbol{\tau}_{\mathrm{lt}}^{\mathrm{btm}}$) are different from the basic field ($\boldsymbol{D}_{\mathrm{b}}$ and $\boldsymbol{\tau}_{\mathrm{b}}^{\mathrm{btm}}$). As a result, when tides are omitted (i.e. $\eta_0 \equiv 0$), $\boldsymbol{U}_{\mathrm{lt}}, \eta_{\mathrm{lt}}, \boldsymbol{D}_{\mathrm{lt}}$ and $\boldsymbol{\tau}_{\mathrm{lt}}^{\mathrm{btm}}$ are permanently zero from Eqs. (11), (12) and (18), so that Eq. (19) becomes identical to the original barotropic equation, Eq. (3). This means that introduction of the tide scheme does not modify the basic equations in contrast to conventional tide schemes.

From a point of view of tide modeling, this scheme enables us to tune the parameters of tides independently of the dynamical balance in the basic field. The value of α and the parameterization of $\boldsymbol{D}_{\mathrm{lt}}$ can be selected arbitrarily. The formulation of $\boldsymbol{\tau}_{\mathrm{lt}}^{\mathrm{btm}}$ can be also decided independently. For example, the constants C_{D} and θ in Eq. (15) can be set different from those of the basic equation, and even a bottom friction formulation different from the basic equation can be adopted for tides. Such use of different bottom friction parameterizations is rational, since turbulent characteristics of the tidal bottom boundary layer are different from those of the bottom boundary layer induced by geostrophic currents (Sakamoto and Akitomo, 2008, 2009).

OSD
10, 473–517, 2013

To clarify the base of the new scheme, the meaning of "the linear tidal component" is noted again here. As shown by Eqs. (11) and (12), the linear tidal component is basically independent of the basic component, though, strictly speaking, a part of the basic component (η) is used in the equations. In other words, the scheme calculates the linear tidal currents under the equilibrium tide potential progressively, and uses it as a model forcing, instead of introducing the potential to the model directly. That is, the linear tidal component can be referred as an external forcing for the model, rather than the tidal field reproduced in the model. To see the tidal field precisely, secondary oscillations with tidal frequencies in the basic field need to be taken into account, as explained in Appendix A.

In closing this subsection, the practical approximation used by the new scheme is discussed in detail in comparison to the scheme of Arbic et al. (2010). The first principle of the new scheme is the fact that the different sets of the governing equations should be applied to the tidal component and the non-tidal component separately, in order to introduce tides into OGCM realistically. And, to do so, we have to carry out decomposition of the two components in OGCM. In an ideal scheme, the tidal component would represent all of the barotropic motions which oscillate with tidal frequencies and have the spatial structures corresponding to the tidal forcing, while the non-tidal component would represent all of the other motions. Hereafter, we call them as "the ideal tidal component" and "the ideal basic component", respectively. Under such an ideal decomposition, the barotropic equation comparable to Eq. (19) becomes

$$\frac{\partial \boldsymbol{U}}{\partial t} + f\boldsymbol{k} \times \boldsymbol{U} = -g(\eta + H)\nabla(\eta_{\mathrm{IB}} + \alpha\eta_{\mathrm{IT}} - \beta\eta_0) + \boldsymbol{D}_{\mathrm{IB}} + \boldsymbol{D}_{\mathrm{IT}} + \boldsymbol{\tau}_{\mathrm{IB}}^{\mathrm{btm}} + \boldsymbol{\tau}_{\mathrm{IT}}^{\mathrm{btm}} + \boldsymbol{X}_{\mathrm{IB}} + \boldsymbol{X}_{\mathrm{IT}}, \tag{20}$$

where the variables with the subscripts of "IB" and "IT" indicate the ideal basic component and the ideal tidal component, respectively. However, it is virtually impossible to extract the ideal tidal component, i.e. all of the motions with tidal frequencies and with spatial patterns corresponding to the tidal forcing, from changing model results. A certain approximation is necessary for the decomposition.

OSD
10, 473–517, 2013

A practical scheme to introduce explicit tidal forcing into OGCM

K. Sakamoto et al.

In the scheme of Arbic et al. (2010), the decomposition is executed somewhat straightforward under limited numerical resources. They approximated terms in Eq. (20) as follows

$$\begin{cases} \eta_{\mathrm{IB}} = \eta_{\text{dynamic-height}} \\ \eta_{\mathrm{IT}} = \eta - \eta_{\text{dynamic-height}} \\ \boldsymbol{D}_{\mathrm{IB}} = \boldsymbol{D}_{25\,\text{h-mean-current}} \\ \boldsymbol{D}_{\mathrm{IT}} = \boldsymbol{D}_{\text{anomaly-current}} \end{cases}, \tag{21}$$

where $\eta_{\text{dynamic-height}}$ indicates the dynamic height anomaly, $\boldsymbol{D}_{25\,\text{h-mean-current}}$ the viscosity for the 25-h mean currents, and $\boldsymbol{D}_{\text{anomaly-current}}$ the viscosity for the anomalous currents. It is guessed that the bottom friction $\boldsymbol{\tau}^{\mathrm{btm}}$ and the other (non-linear) term $\boldsymbol{X}$ are formulated in the same manner for the two components. In OGCM with their tide scheme, Eq. (20) is calculated under these approximations.

Meanwhile, our new scheme approximates terms of Eq. (20) as follows

$$\begin{cases} \eta_{\mathrm{IB}} = \eta_{\mathrm{b}} = \eta - \eta_{\mathrm{lt}} \\ \eta_{\mathrm{IT}} = \eta_{\mathrm{lt}} \\ \boldsymbol{D}_{\mathrm{IB}} = \boldsymbol{D}_{\mathrm{b}} \quad (\text{for } \boldsymbol{U}_{\mathrm{b}} = \boldsymbol{U} - \boldsymbol{U}_{\mathrm{lt}}) \\ \boldsymbol{D}_{\mathrm{IT}} = \boldsymbol{D}_{\mathrm{lt}} \quad (\text{for } \boldsymbol{U}_{\mathrm{lt}}) \\ \boldsymbol{\tau}_{\mathrm{IB}}^{\mathrm{btm}} = \boldsymbol{\tau}_{\mathrm{b}}^{\mathrm{btm}} \quad (\text{for } \boldsymbol{U}_{\mathrm{b}}) \\ \boldsymbol{\tau}_{\mathrm{IT}}^{\mathrm{btm}} = \boldsymbol{\tau}_{\mathrm{lt}}^{\mathrm{btm}} \quad (\text{for } \boldsymbol{U}_{\mathrm{lt}}) \\ \boldsymbol{X}_{\mathrm{IB}} = \boldsymbol{X} \quad (\text{for } \boldsymbol{U}_{\mathrm{b}} + \boldsymbol{U}_{\mathrm{lt}}) \\ \boldsymbol{X}_{\mathrm{IT}} = 0 \end{cases}, \tag{22}$$

by introducing the barotropic linear tidal component, η_{lt} and $\boldsymbol{U}_{\mathrm{lt}}$, and the equations to calculate their time evolution, Eqs. (11) and (12). That is, the practical approximation of the new scheme is to use the solution of a linear tide model in the decomposition. Attributed to this approximation, tidal fields can be reproduced by small numerical resources accurately enough to represent tidal effects on OGCM, as shown in Sect. 3.

OSD
10, 473–517, 2013

However, it may be difficult to reproduce tidal fields in detail in coastal areas, since non-linear effects become important there so that the linear tidal component becomes less representative.

Though small, some numerical resources are expended by the scheme. Since one more barotropic equation needs to be calculated as shown in Fig. 1, the numerical cost of the barotropic calculation doubles. For our test experiment, the computational time increased by 4 % as a whole.

2.3 Model

Test experiments of the tide scheme were executed using the Meteorological Research Institute Community Ocean Model (MRI.COM) (Tsujino et al., 2011). The MRI.COM is a hybrid z-σ coordinate free-surface multilevel model which solves the primitive equations under the hydrostatic and Boussinesq approximations, and adopts a barotropic-baroclinic mode splitting technique. The model domain is global (so called tripolar grid coordinate). The horizontal resolution is 1° in the zonal direction and 1/2° in the meridional direction, except for the Arctic region. The model has 50 levels in the vertical direction with layer thickness increasing from 4 m at the surface to 600 m at 6300-m depth. The model settings are ordinary as recent global OGCMs except for the tide scheme, as summarized in Tsujino et al. (2010). The model uses an isopycnal diffusion, the Second Order Moment tracer advection, a harmonic friction with a Smagorinsky-like viscosity (Griffies and Hallberg, 2000), a sea ice model (Mellor and Kantha, 1989; Hunke and Ducowicz, 1997, 2002), a bottom boundary layer scheme (Nakano and Suginohara, 2002), and the Generic Length Scale vertical mixing scheme (Umlauf and Burchard, 2003). The bottom friction for the basic field, $\boldsymbol{\tau}_{\mathrm{b}}^{\mathrm{btm}}$, is represented by the quadratic friction Eq. (15) with $C_{\mathrm{D}} = 0.00125$ and $\theta = 10°$ (Weatherly et al., 1980).

Configurations of the tide scheme are rather simple in order to verify its basic features. The SAL term is approximated by the linear form $\eta_{\mathrm{SAL}} = (1-\alpha)\eta_{\mathrm{lt}}$ with $\alpha = 0.88$, and the constant β by 0.7. (Strictly speaking, β should depend on the Love numbers.) A simple harmonic horizontal viscosity is used for the diffusivity term $\boldsymbol{D}_{\mathrm{lt}}$ with a

OSD
10, 473–517, 2013

coefficient of $6 \times 10^4\ \mathrm{m^2\,s^{-1}}$, though more sophisticated parameterizations have been proposed such as a formulation dependent on the mixing length (Schwiderski, 1980) and a parameterization for topographic wave drag (Arbic et al., 2004). The no-slip condition is imposed at the lateral boundary of the bottom topography, so that the horizontal viscosity works there. The bottom friction for the linear tidal component $\boldsymbol{\tau}_{\mathrm{lt}}^{\mathrm{btm}}$ is the quadratic friction with the conventional parameters $C_{\mathrm{D}} = 0.0025$ and $\theta = 0^{\circ}$ (Schwiderski, 1980), which are different from $\boldsymbol{\tau}_{\mathrm{b}}^{\mathrm{btm}}$. The main eight tidal constituents (K1, O1, P1, Q1, M2, S2, N2 and K2) are used for the equilibrium tide potential, and their amplitudes and phases are given after Table 1 of Schwiderski (1980). (Two misprints were found: the correct astronomical argument of P1 is $-h_0 - 90$, and the day number from the reference date D is $d + 365(y - 1975) + \mathrm{Int}[(y - 1973)/4]$.)

2.4 Experimental cases

The test experiments were executed under the following boundary and initial conditions. The atmospheric forcings, such as wind stress, latent and sensible heat fluxes, evaporation and precipitation, were calculated using the interannual dataset of the Coordinated Ocean-ice Reference Experiments (Griffies et al., 2009) and the bulk formulas of Large and Yeager (2004). For spin up, we ran the model without tides over one thousand years under the repeated atmospheric forcings from a state of rest with climatological temperature and salinity, to reach a quasi-steady realistic situation (Tsujino et al., 2011). The instantaneous field on 11 May 2001 was used for the initial condition of the tide experiment. The test period was 40 days, though 10 days in some experimental cases. The time step interval is as short as 3 min following Sect. 4b of Schwiderski (1980).

The seven experiment cases were executed (Table 1). The cases TIDE and NOTIDE are with the eight tidal constituents and without tide, respectively, and are mainly analyzed in this paper. The case TIDEa1 with $\alpha = 1$ is used for comparison to show performance of the tide scheme, since it corresponds to a case that the SAL term

OSD
10, 473–517, 2013

A practical scheme to introduce explicit tidal forcing into OGCM

K. Sakamoto et al.

is ignored as in a conventional scheme not to violate dynamical balances in the basic field. (This case does not correspond perfectly to a case using the conventional scheme where tidal and basic fields are treated without separation, since $\boldsymbol{D}_{\mathrm{lt}}$ differs from $\boldsymbol{D}_{\mathrm{b}}$.) The cases M2 and K1 with the single M2 constituent and the K1 constituent, respectively, are used for dynamical analysis of tides in the model. The cases M2d2 and M2d10 changing the tidal horizontal viscosity to $2 \times 10^4\ \mathrm{m}^2\,\mathrm{s}^{-1}$ and $10 \times 10^4\ \mathrm{m}^2\,\mathrm{s}^{-1}$, respectively, are used to examine dependency on the $\boldsymbol{D}_{\mathrm{lt}}$ setting.

The global tide dataset of Matsumoto et al. (2000) (NAO.99b) was downloaded from web and used to assess model reproducibility of the tidal height. This dataset is a reanalysis product made by assimilation of SSH satellite observations to a barotropic tide model with a horizontal resolution of 0.5°. Though they reported that errors in tidal height are 2 cm at maximum (Figs. 3 and 4 of their paper), the dataset is referred as true in this study.

3 Results

3.1 Tidal height

The test experiments with the tide scheme reproduced successfully time evolution of tides as well as the basic field. Figure 2a shows the instantaneous field of SSH η at the end of case TIDE. Tides with a basin scale are clearly seen, along with geostrophic gradients with a large scale, e.g. the meridional gradient of the Antarctic Circumpolar Current.

In this paper, we define the tidal height η_{t} by the SSH anomaly from case NOTIDE,

$$\eta_{\mathrm{t}} \equiv \eta - \eta(\mathrm{NOTIDE}). \tag{23}$$

Figure 2b and c show η_{t} and the linear tidal component η_{lt} in case TIDE, respectively. As noted in Sect. 2.2, the former represents the whole tidal motion including non-linear effects, while the latter the primary barotropic response to the tidal forcing following

OSD
10, 473–517, 2013

Eqs. (11) and (12). Except for a few differences in coastal areas (10 cm at maximum), they are almost identical, at least as for the global distribution (Fig. 2d). This result supports our expectation that the linear tidal component, $\boldsymbol{U}_{\mathrm{lt}}$ and η_{lt}, represents most of the tidal motions. Only the linear tidal equations adopt parameterizations specified for tides in the new scheme, which seems enough to reproduce tides in a global model.

For comparison, Fig. 2e shows the tidal height of the reanalysis dataset (Matsumoto et al., 2000), $\eta_{\mathrm{t}}^{\mathrm{a}}$. The patterns of sea surface elevation in η_{t} (or η_{lt}) of TIDE and $\eta_{\mathrm{t}}^{\mathrm{a}}$ are very similar in the Indian, Pacific and Atlantic oceans, though there are some differences around the Antarctic continent. Their amplitudes are also very close. For example, the local maximum in the eastern equatorial Pacific region is approximately 87 cm in both of η_{t} and $\eta_{\mathrm{t}}^{\mathrm{a}}$. The result indicates that the new scheme worked as expected, so that the model reproduced realistic time evolution of tides.

In contrast, η_{t} in case TIDEa1, which ignored the SAL term, is apparently different from $\eta_{\mathrm{t}}^{\mathrm{a}}$ (Fig. 2f). For example, the local maximum in the east Pacific was not located in the equatorial region, but adjacent to the west coast of North America, and the pattern of sea surface elevation around New Zealand deviated anti-clockwise by approximately 60°. The contrasting results of TIDE and TIDEa1 indicate that realistic tides cannot be modeled in OGCM if the original barotropic equation is used to calculate time evolution of tides. It is necessary to use parameterizations developed for tides, such as the SAL term, as most of barotropic tide models have used.

To investigate causes of the differences between TIDE and TIDEa1 in detail, the amplitude of the tidal height variation is evaluated by the root-mean-square of η_{t}, η_{RMS},

$$\eta_{\mathrm{RMS}} = \left(\frac{1}{T_1 - T_0} \int_{T_0}^{T_1} \eta_{\mathrm{t}}^2 \mathrm{d}t \right)^{1/2}, \tag{24}$$

where T_0 and T_1 indicate 5 May 2001 and 20 June 2001, i.e. the times after 10 and 40 days from the experiment start, respectively. Figure 3 shows η_{RMS} in TIDE, TIDEa1 and the assimilation dataset. In comparison between η_{RMS}(TIDE) and the assimilation

OSD
10, 473–517, 2013

result η^{a}_{RMS}, the distributions and the local maxima are very similar except for some differences (e.g. η_{RMS} is slightly smaller in the Indian Ocean, and larger in the western equatorial Pacific region). Similarly, η_{RMS}(TIDEa1) is close to η^{a}_{RMS}, though its distribution seems somewhat distorted. Thus, it can be concluded that the reproducibility of the tidal height amplitudes is at the same level in TIDE and TIDEa1. This is probably because the two cases use the same viscosity parameterization for tides. (If TIDEa1 had used the original viscosity parameterization of the OGCM, the results would have changed subsequently. See Sect. 3.2.)

Next, the reproducibility of the tidal phase is examined. As a typical result, Fig. 4a shows a time series of η_t at some location in the equatorial Pacific. In contrast to the amplitudes, reproducibility of the tidal phase differs substantially between TIDE and TIDEa1. The η_t phase is ahead by up to 1.5 h from η^{a}_{t} in TIDEa1 (corresponding to 45° for semi-diurnal tides), while by only 0.5 h in TIDE. As a result, the difference between η_t and η^{a}_{t} decreases drastically in TIDE, in comparison with TIDEa1. Thus, the problem that the tidal phase is ahead too much in TIDEa1 is corrected to some extent in TIDE. This is the reason of the difference in the reproducibilities of the two cases shown in Fig. 2.

A possible mechanism of this correction is as follows. Introduction of the SAL term modifies the gravitational acceleration to αg virtually in TIDE, as indicated by Eq. (19). Since α is less than unity (0.88 in our settings), the phase velocity of shallow gravitational waves ($\sqrt{\alpha g/H}$) becomes slower. This mechanism may contribute to reproducibility of the tidal phase.

Additionally, η_t(TIDE) and η^{a}_{t} are shown for 8 days in Fig. 4b. Amplitude modulation induced by neap and spring tides is also well reproduced in the model.

The reproducibility of the tidal height is evaluated quantitatively at the last of this subsection. For this purpose, the root-mean-square error of η_t, η_{RMSE}, is calculated

OSD
10, 473–517, 2013

using η_t^a as a reference (Fig. 5),

$$\eta_{\mathrm{RMSE}} \equiv \left(\frac{1}{T_1 - T_0} \int_{T_0}^{T_1} \left(\eta_t - \eta_t^a \right)^2 \mathrm{d}t \right)^{1/2} . \tag{25}$$

In TIDE, η_{RMSE} is less than 20 cm even in the open oceans where η_{RMS} is large, and less than 10 cm in most of other regions except for around the Antarctic continent. Meanwhile, in TIDEa1, η_{RMSE} is more than 20 cm in most regions so that it reaches comparable to η_{RMS} itself.

As in Arbic et al. (2004), who developed a highly-tuned two-layer tide prediction model without a data assimilation technique, the root-mean-square error is averaged over the region A ranging from 66° S to 66° N with water depth exceeding 1000 m,

$$\overline{\eta}_{\mathrm{RMSE}} \equiv \left(\frac{1}{A} \iint_A \eta_{\mathrm{RMSE}}^2 \mathrm{d}x\mathrm{d}y \right)^{1/2} . \tag{26}$$

The value is up to 31.3 cm in TIDEa1, while 10.0 cm in TIDE, which is comparable to 8.9 cm in Arbic et al. (2004) (Table 2). In addition, Arbic et al. (2004) defined "a percentage of SSH variance captured" by $1 - (\overline{\eta}_{\mathrm{RMSE}}/\overline{\eta}_{\mathrm{RMS}}^a)^2$, where $\overline{\eta}_{\mathrm{RMS}}^a = 31.8$ cm is η_{RMS}^a averaged over A. The values are 90 % in TIDE, 2 % in TIDEa1, and 92 % in Arbic et al. (2004). Thus, the tide reproducibility is very low in TIDEa1, while it increases in TIDE to the same level as the highly-tuned tide model, due to taking into account the SAL term. Since a simple viscosity parameterization was used in the experiment, the reproducibility could increase farther by adopting more sophisticated parameterizations or tuning the settings more carefully. Though this task is beyond the scope of this paper, some case studies shown in Sect. 3.2 indicate that the tide reproducibility significantly depends on the viscosity settings.

OSD
10, 473–517, 2013

3.2 Tidal motion

In this subsection, tidal motions reproduced by the new tide scheme are validated using the results of cases M2 and K1. As shown in Fig. 2, most of the tidal height variation was represented by the linear tidal component η_{lt} in our global model. Similarly, barotropic currents with tidal frequencies were almost represented by the linear tidal component $\boldsymbol{U}_{\mathrm{lt}}$, and therefore $\boldsymbol{U}_{\mathrm{lt}}$ is used to compare with past tide studies. Hereafter, the 100-h experimental results from 20:00 on 5th day (indicated by T_0) to 0:00 on 10th day (T_1) are used for analysis.

As a first step to validate the tidal currents in cases M2 and K1, Fig. 6 shows the mean speed distributions of the barotropic tidal currents $\overline{|\boldsymbol{u}_{\mathrm{lt}}|}^{t}$ calculated by

$$\overline{|\boldsymbol{u}_{\mathrm{lt}}|}^{t} = \frac{1}{T_1 - T_0}\int_{T_0}^{T_1} \left| \frac{\boldsymbol{U}_{\mathrm{lt}}}{H+\eta} \right| \mathrm{d}t. \tag{27}$$

The tidal currents are strong in coastal areas, especially Great Britain and Ireland and far east Asia, commonly in the both cases. In open oceans, $\overline{|\boldsymbol{u}_{\mathrm{lt}}|}^{t}$ is large over the Mid Atlantic Ridge and in the equatorial Pacific in M2, while in the Indian Ocean and the North Pacific in K1. Including these characteristics, the distributions agree well with Fig. 1 of Müller et al. (2010).

Next, we executed an energy analysis for the M2 tide. Generally, the tide energy is supplied to the ocean in interior regions of basins, and then transported to narrow coastal regions to be dissipated there. Egbert and Ray (2003) analyzed the path ways of the M2 tide energy based on an assimilation model. Following them, the tide energy flux $\boldsymbol{P}$ and the energy supply W (i.e. the work which the tide forcing does against the

OSD
10, 473–517, 2013

ocean) are estimated for the linear tidal component,

$$\boldsymbol{P} = \frac{1}{T_1 - T_0} \int_{T_0}^{T_1} \boldsymbol{U}_{\mathrm{lt}} \eta_{\mathrm{lt}} \mathrm{d}t \tag{28}$$

$$W = \frac{1}{T_1 - T_0} \int_{T_0}^{T_1} \boldsymbol{U}_{\mathrm{lt}} \cdot \nabla(\beta \eta_0 + \eta_{\mathrm{SAL}}) \mathrm{d}t. \tag{29}$$

See Sect. 3.1 of Egbert and Ray (2001) for derivation of Eqs. (28) and (29). Figure 7 verifies that the energy was supplied in interior regions and transported to coastal regions. In addition, the $\boldsymbol{P}$ vector map agrees well with Egbert and Ray (2001). These results indicate that our model reproduced not only the tidal heights, but also tidal dynamics such as the tidal currents and the energy flux, which are important for effects on the basic fields.

It has been shown that precision of a tide model depends primarily on settings of viscosity and friction to dissipate tidal currents (Arbic et al., 2004). Also in our model experiments, tides significantly depended on the viscosity settings, especially the horizontal viscosity ν. Figure 8 shows η_{t} in the two additional cases where ν was decreased to $2 \times 10^4\ \mathrm{m}^2\,\mathrm{s}^{-1}$ (case M2v2) and increased to $10 \times 10^4\ \mathrm{m}^2\,\mathrm{s}^{-1}$ (M2v10), together with the standard case with $\nu = 6 \times 10^4\ \mathrm{m}^2\,\mathrm{s}^{-1}$. Though the patterns of sea surface elevation were similar, the magnitudes differed significantly, e.g. the local maxima in the eastern equatorial Pacific of 84 cm, 63 cm and 52 cm in cases M2v2, M2 and M2v10, respectively. In addition, it was revealed that the amplitudes of tidal height variation were mainly controlled by the viscosity on the lateral boundary of bottom topography, rather than the horizontal viscosity between interior currents or bottom friction (not shown). These results are consistent with Schwiderski (1980) and Arbic et al. (2004), who reported that interaction between tidal currents and bottom topography is one of the most important processes in dissipation of tides. As noted here, by using the new scheme,

OSD
10, 473–517, 2013

we could adjust the tide viscosity and friction parameters including interaction between tides and topography, independently of the original OGCM equations. This feature is essential to introduce tides into OGCM realistically, as Arbic et al. (2010) pointed out.

3.3 Effects on basic fields

As noted in Sect. 2.2, the new tide scheme is designed so that interaction processes between the basic fields and tides are represented in the original OGCM framework. Owing to this, the tidal effects on the basic fields would be reproduced naturally in the model, as long as the tidal currents are generated realistically by the scheme. Therefore, we expected that some reasonable changes happened in the velocity and tracer fields of the test experiments, since the tidal currents were well reproduced. In order to validate impacts of the tide scheme, changes in the basic fields are summarized briefly in this subsection, though the experimental period (40 days) and the model resolution ($1^\circ \times 1/2^\circ$) are not enough to represent thorough modification of the basic fields in the real ocean.

In general, active excitement of internal waves is one of the main impacts of tides on the basic fields. Figure 9 shows vertical velocity w at the depth of 1900 m in cases TIDE and NOTIDE. In NOTIDE, w was $O(10^{-3})\,\mathrm{cm\,s^{-1}}$ except for the equatorial region, while more than $10^{-2}\,\mathrm{cm\,s^{-1}}$ over large areas in TIDE. This difference indicates excitement of internal tides in TIDE. In fact, the vertical velocity was especially large over rough topographies such as the Emperor Seamount Chain (near 170° E), the Hawaiian Ridge and the Izu-Ogasawara Ridge (140° E), suggesting active excitement due to interaction between tides and topographies.

Figure 9 shows that w had a zonal band pattern with a meridional wavelength of approximately 200 km. This pattern is very similar to the result of Komori et al. (2008) (their Fig. 1), who simulated excitement of internal waves by wind using a model with a horizontal resolution of 1/4°. However, Arbic et al. (2010) reported that internal tides have a ripple-like pattern spreading from bottom topographies, using an eddy-resolving model with a horizontal resolution of approximately 1/10°. Since reproducibility of

OSD
10, 473–517, 2013

internal tides depends sharply on model resolution (Niwa and Hibiya, 2011), this difference suggests that our model resolution of $1^\circ \times 1/2^\circ$ was not enough to represent internal tides.

As another impact on the ocean, Fig. 10a shows sea surface temperature (SST) anomaly $\Delta\overline{T}^{t}$,

$$\Delta\overline{T}^{t} = \overline{T}^{t}(\mathrm{TIDE}) - \overline{T}^{t}(\mathrm{NOTIDE}), \tag{30}$$

where $\overline{T}^{t}$ indicates the last 25-h mean temperature (in 19 June). Introduction of tides resulted in SST decrease by 0.1–0.5° C over large areas of the Northern Hemisphere. As shown by a vertical temperature profile (Fig. 10b), the surface layer of 0–15 m became cooler, while the subsurface layer of 20–40 m warmer, and the temperature stratification was weakened. That is, development of the thermocline in subtropical and subpolar regions of the Northern Hemisphere was hampered, and as a result, SST increase in early summer was weakened. This is likely attributed to the process that vertical shear in internal tides feeds vertical mixing in the surface layer through the vertical mixing scheme. Actually, the mixing scheme predicted large vertical diffusivity intermittently. In contrast, $\Delta\overline{T}^{t}$ was small in the Southern Hemisphere of winter. It is thought that tidal mixing affected hardly vertical temperature distribution there, since the surface layer was originally well mixed due to surface cooling (both of temperature and salinity were almost uniform from the surface to the depth of 80 m).

SST decrease was especially large in shallow coastal regions, such as more than 1° C around the islands of Great Britain and Ireland. Since this decrease was accompanied with weakening of stratification as in open oceans of the Northern Hemisphere, the reason is likely that strong tidal currents (Fig. 6) induced vertical mixing through shear instability in the bottom layer, as reported by observational and numerical studies about tidal fronts (Simpson and Hunter, 1974; Müller et al., 2010). The SST anomaly was also large in some polar coastal seas such as the Greenland Sea and the Ross Sea. This

OSD
10, 473–517, 2013

seems to support past studies which showed significant tidal impacts on dense water formation processes there (Pereira et al., 2002; Robertson, 2001a,b).

Our experiment of 40 days did not show any significant changes in large scale circulations. The residual currents were less than $1\,\mathrm{cm\,s^{-1}}$ in the open oceans, and $10\,\mathrm{cm\,s^{-1}}$ at maximum in coastal areas (not shown). This result is consistent with a study about tidal effects (Bessiéres et al., 2008), which suggests that the new tide scheme did not generate apparently irrational currents. However, considering the report that tidal mixing modified the Atlantic North Current pathway in a long-term integration of a climate model (Müller et al., 2010), tidal impacts on large scale circulations may appear if we run the model much longer.

Though plausible results were obtained by the new scheme as for impacts of tidal currents, it should be noted that the experiment is preliminary. In particular, the horizontal resolution of the model is too low to represent internal tides or tidal mixing processes (Matsumoto et al., 2000). A thorough investigation is necessary about the process for tidal currents to intensify vertical mixing through velocity shear and turbulence. We plan to execute a long experiment in order to examine the tidal impacts in more detail, including dependencies on model resolution or mixing parameterizations.

4 Conclusions

A new practical scheme is proposed to introduce tides explicitly into ocean general circulation models (OGCM). In this scheme, barotropic linear response to the tidal forcing is calculated by the time differential equations modified for ocean tides, instead of the original barotropic equations of OGCM. This allows usage of various parameterizations specified for tides, such as the self attraction/loading (SAL) effect and energy dissipation due to internal tides, without unintentional violation of the original dynamical balances in OGCM. Owing to this feature, the knowledge of barotropic tide modeling can be exploited to improve reproducibility of tides in OGCM. In other words, this scheme drives OGCM by the barotropic tidal currents which are predicted progressively by

OSD
10, 473–517, 2013

a well-tuned tide model, instead of the equilibrium tide potential. The numerical cost of the scheme is comparable to the barotropic calculation of the original OGCM.

We incorporated this scheme into Meteorological Research Institute Community Ocean Model (MRI.COM) and executed test experiments with a low-resolution global model ($1^\circ \times 1/2^\circ$). The results showed that the model could simulate tides realistically without affecting the basic fields unintentionally. The root mean square error of the tidal heights was only 10.0 cm in the reference of a data-assimilation result, indicating that the tide reproducibility is comparable to that of tide models tuned elaborately. In contrast, in the case that the SAL term was ignored, the reproducibility decreased significantly as the error was up to 31.3 cm. This indicates that parameterizations specified for tides must be utilized in order to introduce tides into OGCM realistically. Although this statement has been pointed out by Arbic et al. (2010), our methodology is different from theirs.

It should be noted that our model settings were rather crude. Recently, sophisticated parameterizations for tidal energy dissipation have been proposed by studies about interaction between tides and topography (e.g. Jayne and St. Laurent, 2001). The tide reproducibility may improve further by adopting such parameterizations, making use of the feature that the tide settings can be decided independently of OGCM. Actually, our case studies showed that the reproducibility depends sharply on the configuration of the viscosity related to topography, suggesting a possible contribution of such parameterizations.

In spite of the crude settings, our model reproduced the amplitudes of the M2 and K1 tidal currents and the conversion process of tide energy, in the fashion reported by tide modeling studies. In addition, excitement of internal tides and enhancement of vertical mixing were also realistic in the model, though the experimental period was as short as 40 days. These results mean that the scheme generated the realistic tidal currents in the model, and that the model explicitly reproduced processes for current shear to enhance vertical mixing. This is in contrast to the indirect parameterizations of tidal mixing used by many traditional OGCMs, such as additional increase of the

OSD
10, 473–517, 2013

background vertical diffusivity. Advection by the tidal currents is also treated explicitly in the model with this scheme. Usage of the scheme is expected to improve representation of various physical processes such as water exchange between coastal and open oceans, and even chemical and biological processes. Explicit introduction of tides into OGCM is a significant step toward upgrade of ocean modeling. We have a plan to investigate the impacts in more detail using a model with a finer resolution.

Appendix A

Modification of tides

Tides affect the basic field as shown in Sect. 3.3, and also the basic field modifies tides in turn. For example, when density stratification exists, kinetic energy conversion occurs from barotropic tides to internal tides. In the new tide scheme, the linear tidal component represents the primary barotropic response to the equilibrium tide potential, and does not include such modification. This Appendix explains how such modification is represented in the framework of the new tide scheme.

To treat the question clearly and analytically, we consider a simple situation as follows. The ocean state is thoroughly horizontally uniform including the tidal forcing, and dissipation and bottom friction are ignored. Under these assumptions, the momentum equation of the linear tidal component, Eq. (11), is simplified as

$$\frac{\partial U_{\mathrm{lt}}}{\partial t} - fV_{\mathrm{lt}} = gH\beta\frac{\partial \eta_0}{\partial x} \tag{A1}$$

$$\frac{\partial V_{\mathrm{lt}}}{\partial t} + fU_{\mathrm{lt}} = gH\beta\frac{\partial \eta_0}{\partial y}. \tag{A2}$$

OSD
10, 473–517, 2013

A practical scheme to introduce explicit tidal forcing into OGCM

K. Sakamoto et al.

Now, introducing complex number expressions

$$\boldsymbol{U}_{\mathrm{lt}} = U_{\mathrm{lt}} + iV_{\mathrm{lt}} \tag{A3}$$

$$\boldsymbol{F} = \frac{\partial \eta_0}{\partial x} + i\frac{\partial \eta_0}{\partial y}, \tag{A4}$$

we deform Eqs. (A1) and (A2) into

$$\frac{\partial \boldsymbol{U}_{\mathrm{lt}}}{\partial t} + if\boldsymbol{U}_{\mathrm{lt}} = gH\beta\boldsymbol{F}. \tag{A5}$$

We assume a horizontal vector varying trigonometrically with frequency σ for the tidal forcing $\boldsymbol{F}$, and as a result, each of $\boldsymbol{U}_{\mathrm{lt}}$ and $\boldsymbol{F}$ can be deformed to a sum of the two circular components in general as follows (Davies, 1985; Sakamoto and Akitomo, 2006)

$$\boldsymbol{U}_{\mathrm{lt}} = R_{\mathrm{lt}}^{+}e^{i\sigma t} + R_{\mathrm{lt}}^{-}e^{-i\sigma t} \tag{A6}$$

$$\boldsymbol{F} = F^{+}e^{i\sigma t} + F^{-}e^{-i\sigma t}, \tag{A7}$$

where R_{lt}^{+} and F^{+} are the amplitudes of the anti-clockwise components while R_{lt}^{-} and F^{-} are those of the clockwise components. Substituting Eqs. (A6) and (A7) into Eq. (A5), we obtain the solution of $\boldsymbol{U}_{\mathrm{lt}}$ for $\boldsymbol{F}$,

$$R_{\mathrm{lt}}^{+} = \frac{gH\beta}{i(\sigma+f)}F^{+} \tag{A8}$$

$$R_{\mathrm{lt}}^{-} = \frac{gH\beta}{i(-\sigma+f)}F^{-}. \tag{A9}$$

Now that the solution for the linear tidal component is obtained, we show how the basic equations represent modification of tides induced by secondary interactions between the linear tidal component $\boldsymbol{U}_{\mathrm{lt}}$ and the basic field. Making use of the assumptions

OSD
10, 473–517, 2013

of Eqs. (A1) and (A2), the barotropic momentum equation of the basic component Eq. (13), i.e. the original equation of OGCM , is simplified to

$$\frac{\partial \boldsymbol{U}_\mathrm{b}}{\partial t} + if\boldsymbol{U}_\mathrm{b} = \boldsymbol{X}, \tag{A10}$$

where $\boldsymbol{U}_\mathrm{b}$ is a complex number,

$$\boldsymbol{U}_\mathrm{b} = U_\mathrm{b} + iV_\mathrm{b}, \tag{A11}$$

and $\boldsymbol{X}$ represents the secondary interactions. Here, we assume a linear damping for $\boldsymbol{X}$, modeling the process that the barotropic tides are dissipated by excitation of the internal tides due to combination of tidal currents and stratification,

$$\boldsymbol{X} = -a\boldsymbol{U}_\mathrm{lt}. \tag{A12}$$

The constant a is a damping coefficient with unit of s^{-1}. Now, we deform $\boldsymbol{U}_\mathrm{b}$ to a sum of the two circular components in the same manner as Eq. (A6),

$$\boldsymbol{U}_\mathrm{b} = R_\mathrm{b}^{+}e^{i\sigma t} + R_\mathrm{b}^{-}e^{-i\sigma t}. \tag{A13}$$

Substituting Eqs. (A12) and (A13) into Eq. (A10), we obtain the modification of the tidal currents induced by the secondary interaction $\boldsymbol{X}$ as

$$R_\mathrm{b}^{+} = \frac{-a}{i(\sigma + f)}R_\mathrm{lt}^{+} \tag{A14}$$

$$R_\mathrm{b}^{-} = \frac{-a}{i(-\sigma + f)}R_\mathrm{lt}^{-}. \tag{A15}$$

The actual tidal currents are a sum of the linear tidal component $\boldsymbol{U}_\mathrm{lt}$ and the modification due to the secondary interactions. Since the latter is equal to $\boldsymbol{U}_\mathrm{b}$ in the present

OSD
10, 473–517, 2013
A practical scheme to introduce explicit tidal forcing into OGCM
K. Sakamoto et al.

situation, the entire tidal currents driven by the forcing $\boldsymbol{F}$ are given by Eqs. (A8), (A9), (A14) and (A15) as follows

$$\boldsymbol{U}_{\mathrm{lt}} + \boldsymbol{U}_{\mathrm{b}} = \left(1 + \frac{-a}{i(\sigma+f)}\right)\frac{gH\beta}{i(\sigma+f)}F^{+}e^{i\sigma t} + \left(1 + \frac{-a}{i(-\sigma+f)}\right)\frac{gH\beta}{i(-\sigma+f)}F^{-}e^{-i\sigma t}. \quad \text{(A16)}$$

This expression clearly shows how the tidal currents induced by F^{+} and F^{-} are modified by the dumping a, which represents the secondary interaction between the tidal and basic fields. The relative magnitude of the modification against the linear tidal component is indicated by the ratio of a against $\sigma + f$. This means that the modification is usually smaller than the linear tidal component, since time scales of decay of barotropic tidal currents due to excitement of internal waves (or other interaction processes) are usually larger than periods of main tidal constituents or the inertial period ($\sim$ day). This is consistent with our test experiments, where the tides are almost entirely represented by the linear tidal component (Fig. 2).

As explained here using a simple situation, interaction between the tidal and basic fields emerges as a driving term ($\boldsymbol{X}$) in the basic equation. Change of the basic field induced by $\boldsymbol{X}$ can be considered as modification of tides, if its frequency is same as the tidal forcing. Otherwise, the change is excitation of other tidal constituents such as overtides, or modification of the basic field. In any case, these modification processes are represented explicitly in the framework of the original OGCM, although the governing equations of the modification currents $\boldsymbol{U}_{\mathrm{b}}$ are different from those of the linear tidal currents $\boldsymbol{U}_{\mathrm{lt}}$.

Acknowledgements. We thank the members of oceanographic research department of Meteorological Research Institute for fruitful discussions and helpful comments. This work was funded by MRI and was partly supported by JSPS KAKENHI Grant Number 24740323.

OSD
10, 473–517, 2013

References

Arbic, B. K., Garner, S. T., Hallberg, R. W., and Simmons, H. L.: The accuracy of surface elevations in forward global barotropic and baroclinic tide models, Deep-Sea Res. Pt. II, 51, 3069–3101, doi:10.1016/j.dsr2.2004.09.014, 2004. 477, 487, 491, 493, 507

Arbic, B. K., Wallcraft, A. J., and Metzger, E. J.: Concurrent simulation of the eddying general circulation and tides in a global ocean model, Ocean Model., 32, 175–187, doi:10.1016/j.ocemod.2010.01.007, 2010. 476, 477, 478, 484, 485, 494, 497

Bessiéres, L., Madec, G., and Lyard, F.: Global tidal residual mean circulation: does it affect a climate OGCM?, Geophys. Res. Lett., 35, L03609, doi:10.1029/2007GL032644, 2008. 475, 496

Davies, A. M.: On determining current profiles in oscillatory flows, Appl. Math. Model., 9, 419–428, 1985. 499

Egbert, G. D. and Ray, R. D.: Estimates of M2 tidal energy dissipation from TOPEX/Poseidon altimeter data, J. Geophys. Res., 106, 22475–22502, doi:10.1029/2000JC000699, 2001. 475, 493, 514

Egbert, G. D. and Ray, R. D.: Semi-diurnal and diurnal tidal dissipation from TOPEX/Poseidon altimetry, Geophys. Res. Lett., 30, 1907, doi:10.1029/2003GL017676, 2003. 492

Griffies, S. M. and Hallberg, R. W.: Biharmonic friction with a Smagorinsky-like viscosity for use in large-scale eddy-permitting ocean models, Mon. Weather Rev., 128, 2935–2946, 2000. 486

Griffies, S. M., Biastoch, A., Böning, C., Bryan, F., Danabasoglu, G., Chassignet, E. P., England, M. H., Gerdes, R., Haak, H., Hallberg, R. W., Hazeleger, W., Jungclaus, J., Large, W. G., Madec, G., Pirani, A., Samuels, B. L., Scheinert, M., Gupta, A. S., Severijns, C. A., Simmons, H. L., Treguier, A. M., Winton, M., Yeager, S., and Yin, J.: Coordinated Ocean-ice Reference Experiments (COREs), Ocean Model., 26, 1–26, 2009. 487

Hunke, E. C. and Ducowicz, J. K.: An elastic-viscous-plastic model for sea ice dynamics, J. Phys. Oceanogr., 27, 1849–1867, 1997. 486

Hunke, E. C. and Ducowicz, J. K.: The elastic-viscous-plastic sea ice dynamics model in general orthogonal curvilinear coordinates on a sphere: Incorporation of metric terms, Mon. Weather Rev., 130, 1848–1865, 2002. 486

Jayne, S. R. and St. Laurent, L. C.: Parameterizing tidal dissipation over rough topography, Geophys. Res. Lett., 28, 811–814, 2001. 477, 497

Discussion Paper | Discussion Paper | Discussion Paper | Discussion Paper |

OSD
10, 473–517, 2013

A practical scheme to introduce explicit tidal forcing into OGCM

K. Sakamoto et al.

Kantha, L. H. and Clayson, C. A.: Numerical Models of Oceans and Oceanic Processes, Academic Press, 2000. 477

Komori, N., Ohfuchi, W., Taguchi, B., Sasaki, H., and Klein, P.: Deep ocean inertia-gravity waves simulated in a high-resolution global coupled atmosphere-ocean GCM, Geophys. Res. Lett., 35, L04610, doi:10.1029/2007GL032807, 2008. 494

Large, W. G. and Yeager, S. G.: Diurnal to decadal global forcing for coean and sea-ice models: The data sets and flux climatologies, NCAR Tech. Note: TN-460+STR, CGD Division of the Natinal Center for Atmospheric Research, 2004. 487

Lee, H. C., Rosati, A., and Spelman, M. J.: Barotropic tidal mixing effects in a coupled climate model: oceanic conditions in the Northern Atlantic, Ocean Model., 11, 464–477, 2006. 475

Matsumoto, K., Takanezawa, T., and Ooe, N.: Ocean tide models developed by assimilating TOPEX/POSEIDON altimeter data into hydrodynamical model: a global model and a regional model around Japan, J. Oceanogr., 56, 567–581, 2000. 476, 477, 488, 489, 496

Mellor, G. L. and Kantha, L.: An ice-ocean coupled model, J. Geophys. Res., 94, 10937–10954, 1989. 486

Müller, M., Haak, H., Jüngclaus, J., Sundermann, J., and Thomas, M.: The effect of ocean tides on a climate model simulation, Ocean Model., 35, 304–313, doi:10.1016/j.ocemod.2010.09.001, 2010. 476, 478, 492, 495, 496, 513

Munk, W. and Wunsch, C.: Abyssal recipes II: energetics of tidal and wind mixing, Deep-Sea Res. Pt. I, 45, 1977–2010, 1998. 474

Nakamura, T. and Awaji, T.: Tidally induced diapycnal mixing in the Kuril Straits and its role in water transformation and transport: a three-dimensional nonhydrostatic model experiment, J. Geophys. Res., 109, 07, doi:10.1029/2003JC001850, 2004. 475

Nakano, H. and Suginohara, N.: Effects of Bottom Boundary Layer parameterization on reproducing deep and bottom waters in a world ocean model, J. Phys. Oceanogr., 32, 1209–1227, 2002. 486

Niwa, Y. and Hibiya, T.: Estimation of baroclinic tide energy available for deep ocean mixing based on three-dimensional global numerical simulations, J. Oceanogr., 67, 493–502, doi:10.1007/s10872-011-0052-1, 2011. 475, 477, 495

Osafune, S. and Yasuda, I.: Bidecadal variability in the intermediate waters of the northwestern subarctic Pacific and the Okhotsk Sea in relation to 18.6-year period nodal tidal cycle, J. Geophys. Res., 111, C05007, doi:10.1029/2005JC003277, 2006. 475

OSD
10, 473–517, 2013

A practical scheme to introduce explicit tidal forcing into OGCM

K. Sakamoto et al.

Title Page
Abstract | Introduction
Conclusions | References
Tables | Figures
◀| |▶
◀ ▶
Back | Close
Full Screen / Esc
Printer-friendly Version
Interactive Discussion

Pereira, F. P., Beckmann, A., and Hellmer, H. H.: Tidal mixing in the southern Weddell Sea: results from a three-dimensional model, J. Phys. Oceanogr., 32, 2151–2170, 2002. 475, 496

Postlethwaite, C. F., Morales Maqueda, M. A., le Fouest, V., Tattersall, G. R., Holt, J., and Willmott, A. J.: The effect of tides on dense water formation in Arctic shelf seas, Ocean Sci., 7, 203–217, doi:10.5194/os-7-203-2011, 2011. 475

Robertson, R.: Internal tides and baroclinicity in the southern Weddell Sea 1. Model description, J. Geophys. Res., 106, 27001–27016, 2001a. 475, 496

Robertson, R.: Internal tides and baroclinicity in the southern Weddell Sea 2. Effects of the critical latitude and stratification, J. Geophys. Res., 106, 27017–27034, 2001b. 475, 496

Sakamoto, K. and Akitomo, K.: Instabilities of the tidally induced bottom boundary layer in the rotating frame and their mixing effect, Dyn. Atmos. Oceans, 41, 191–211, 2006. 499

Sakamoto, K. and Akitomo, K.: The tidally induced bottom boundary layer in the rotating frame: Similarity of turbulence, J. Fluid Mech., 615, 1–25, 2008. 483

Sakamoto, K. and Akitomo, K.: The tidally induced bottom boundary layer in the rotating frame: development of the turbulent mixed layer under stratification, J. Fluid Mech., 619, 235–259, 2009. 483

Schiller, A.: Effects of explicit tidal forcing in an OGCM on the water-mass structure and circulation in the Indonesian throughflow region, Ocean Model., 6, 31–49, 2004. 478, 479

Schiller, A. and Fiedler, R.: Explicit tidal forcing in an ocean general circulation model, Geophys. Res. Lett., 34, L03611, doi:10.1029/2006GL028363, 2007. 476, 478

Schwiderski, E. W.: On charting global ocean tides, Rev. Geophys. Space Phys., 18, 243–268, doi:10.1029/RG018i001p00243, 1980. 476, 479, 480, 487, 493

Simpson, J. H. and Hunter, J. R.: Fronts in the Irish Sea, Nature, 250, 404–406, 1974. 495

St. Laurent, L. and Garrett, C.: The role of internal tides in mixing the deep ocean, J. Phys. Oceanogr., 32, 2882–2899, 2002. 475

Thomas, M., Sündermann, J., and Maier-Reimer, E.: Consideration of ocean tides in an OGCM and impacts on subseasonal to decadal polar motion excitation, Geophys. Res. Lett., 28, 2457–2460, 2001. 478

Tsujino, H., Motoi, T., Ishikawa, I., Hirabara, M., Nakano, H., Yamanaka, G., Yasuda, T., and Ishizaki, H.: Reference manual for the Meteorological Research Institute Community Ocean Model (MRI.COM) version 3, Technical reports of the Meteorological Research Institute, 59, 241 pp., http://www.mri-jma.go.jp/Publish/Technical/index_en.html, 2010. 486

OSD
10, 473–517, 2013

A practical scheme to introduce explicit tidal forcing into OGCM

K. Sakamoto et al.

Title Page
Abstract | Introduction
Conclusions | References
Tables | Figures
◂◂ | ▸▸
◂ | ▸
Back | Close
Full Screen / Esc
Printer-friendly Version
Interactive Discussion

Tsujino, H., Hirabara, M., Nakano, H., Yasuda, T., Motoi, T., and Yamanaka, G.: Simulating present climate of the global ocean-ice system using the Meteorological Research Institute Community Ocean Model (MRI.COM): simulation characteristics and variability in the Pacific sector, J. Oceanogr., 67, 449–479, doi:10.1007/s10872-011-0050-3, 2011. 486, 487
Umlauf, L. and Burchard, H.: A generic length-scale equation for geophysical turbulence models, J. Marine Res., 61, 235–265, 2003. 486
Weatherly, G. L., Blumsack, S. L., and Bird, A. A.: On the effect of diurnal tidal currents in determining the thickness of the turbulent Ekman bottom boundary layer, J. Phys. Oceanogr., 10, 297–300, 1980. 482, 486

OSD
10, 473–517, 2013

Title Page
Abstract | Introduction
Conclusions | References
Tables | Figures
◄ | ►
Back | Close
Full Screen / Esc
Printer-friendly Version
Interactive Discussion

Table 1. Experimental cases.

Abbreviation	settings
NOTIDE	without tide
TIDE	8 tidal constituents
TIDEa1	8 tidal constituents, $\alpha = 1$
M2	M2
K1	K1
M2d2	M2, horizontal viscosity $= 2 \times 10^4\ \mathrm{m}^2\,\mathrm{s}^{-1}$
M2d10	M2, horizontal viscosity $= 10 \times 10^4\ \mathrm{m}^2\,\mathrm{s}^{-1}$

OSD
10, 473–517, 2013

Table 2. Reproducibility of the tidal height in TIDE, TIDEa1 and the tide prediction model of Arbic et al. (2004).

Case	TIDE	TIDEa1	Arbic et al. (2004)
Error RMS [cm]	10.0	31.3	8.9
percentage of SSH variance captured [%]	90	2	92

OSD
10, 473–517, 2013

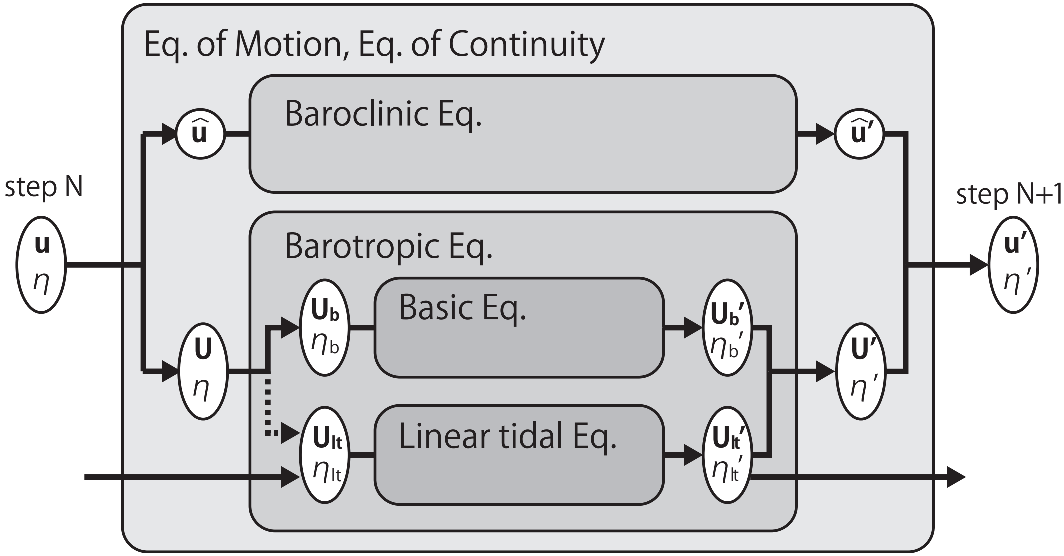

Fig. 1. A schematic view of the calculation procedure of the tide scheme. From $\boldsymbol{u}$ and η at the time step N, $\boldsymbol{u}'$ and η' at the next step $N+1$ are calculated following the equations of motion and continuity. In the calculation process, the mode splitting technique splits the variables into the baroclinic constituent, $\hat{\boldsymbol{u}}$, and the barotropic one, $\boldsymbol{U}$ and η, and then the tide scheme splits the latter into the basic component, $\boldsymbol{U}_\mathrm{b}$ and η_b, and the linear tidal component, $\boldsymbol{U}_\mathrm{lt}$ and η_lt. Each component calculates time evolution ($\hat{\boldsymbol{u}}'$,$\boldsymbol{U}'_\mathrm{b}$,$\eta'_\mathrm{b}$,$\boldsymbol{U}'_\mathrm{lt}$ and η'_lt), and subsequently all of them are summed to obtain $\boldsymbol{u}'$ and η'. The dashed and solid arrows which point to $\boldsymbol{U}_\mathrm{lt}$ and η_lt mean that their time evolution are given almost independently (see the main text).

OSD
10, 473–517, 2013

A practical scheme to introduce explicit tidal forcing into OGCM

K. Sakamoto et al.

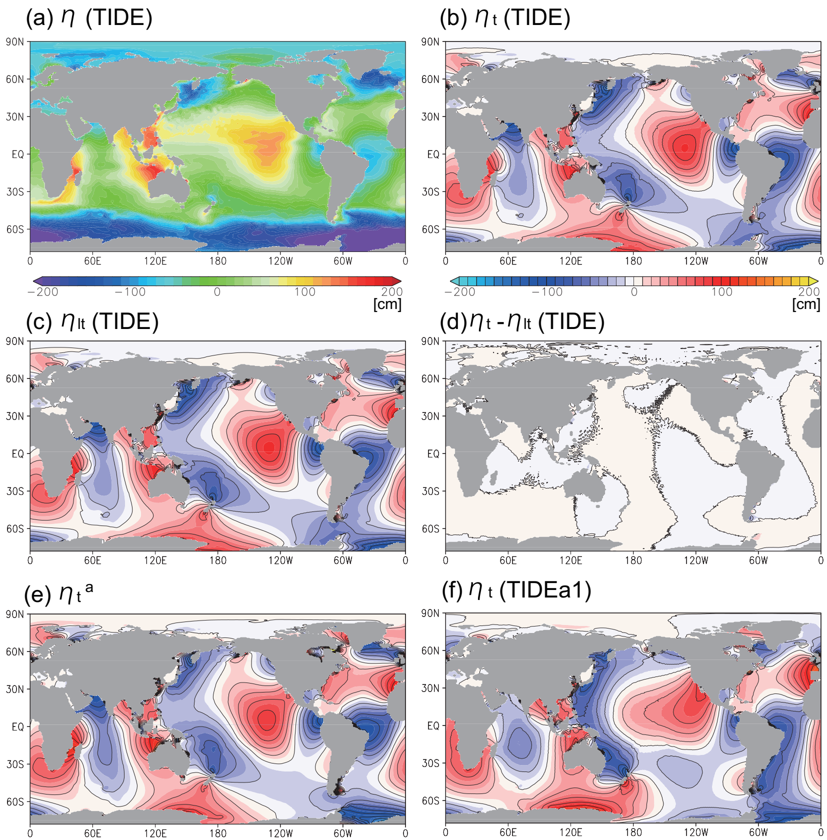

Fig. 2. (a) SSH η, **(b)** tidal height η_t, **(c)** height of the linear tidal component η_{lt}, **(d)** the difference $\eta_t - \eta_{lt}$ in case TIDE, **(e)** data assimilation analysis η_t^a and **(f)** η_t in TIDEa1 at the end of the experiments (20 June 2001 0:00 UTC). The same color shades are used in **(b–f)**, and red indicates ascend (positive) while blue descend (negative). The contour interval is 20 cm.

OSD
10, 473–517, 2013

A practical scheme to introduce explicit tidal forcing into OGCM

K. Sakamoto et al.

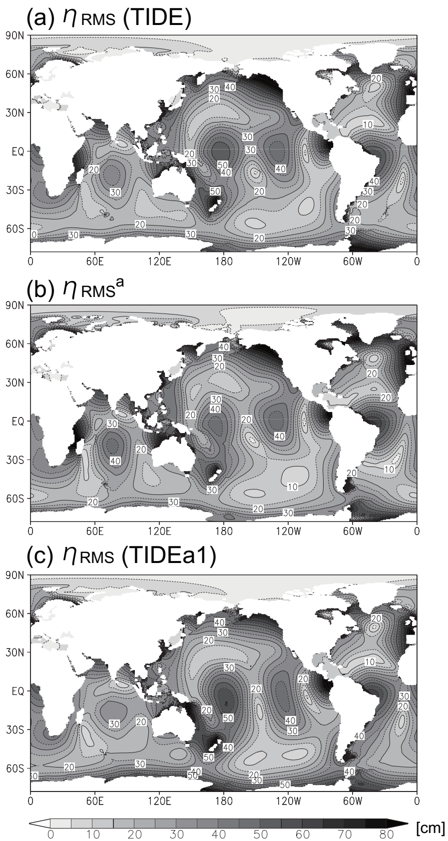

Fig. 3. Root mean square of tidal height η_{RMS} (Eq. 24) in **(a)** TIDE, **(b)** assimilation analysis and **(c)** TIDEa1. The contour interval is 5 cm.

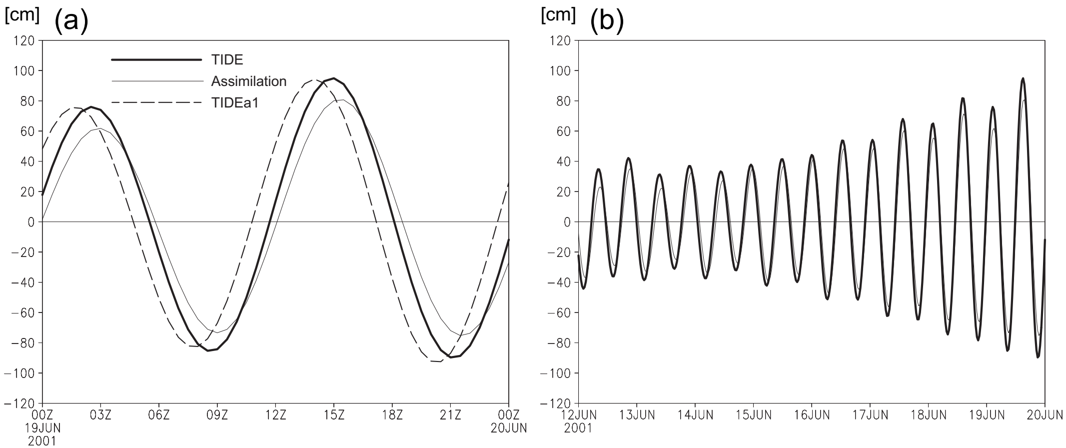

Fig. 4. Time variation of tidal height η_t at the site (180° E, 0° N) for **(a)** 19–20 June 2001 and **(b)** 12–20 June 2001. The thick, thin and dashed lines indicate TIDE, assimilation analysis and TIDEa1, respectively, though TIDEa1 is omitted in **(b)**.

OSD
10, 473–517, 2013

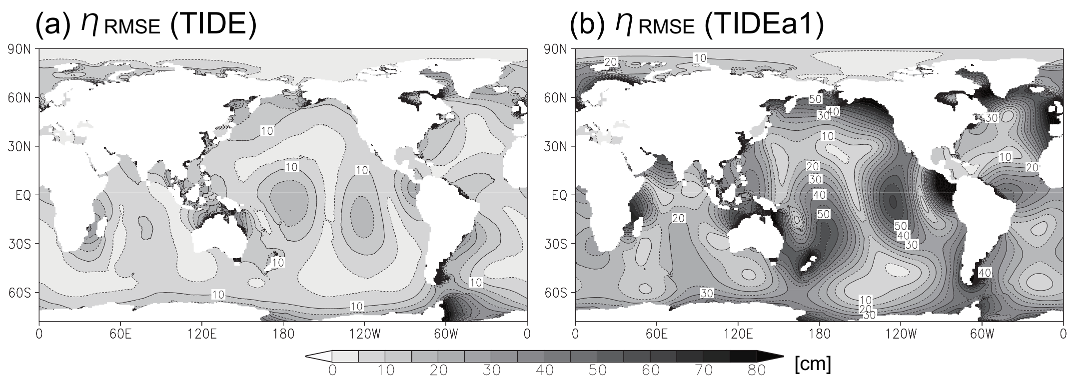

Fig. 5. Root mean square error of the tidal height η_{RMSE} in **(a)** TIDE and **(b)** TIDEa1. The contour interval is 5 cm.

OSD
10, 473–517, 2013

A practical scheme to introduce explicit tidal forcing into OGCM

K. Sakamoto et al.

OSD
10, 473–517, 2013

A practical scheme to introduce explicit tidal forcing into OGCM

K. Sakamoto et al.

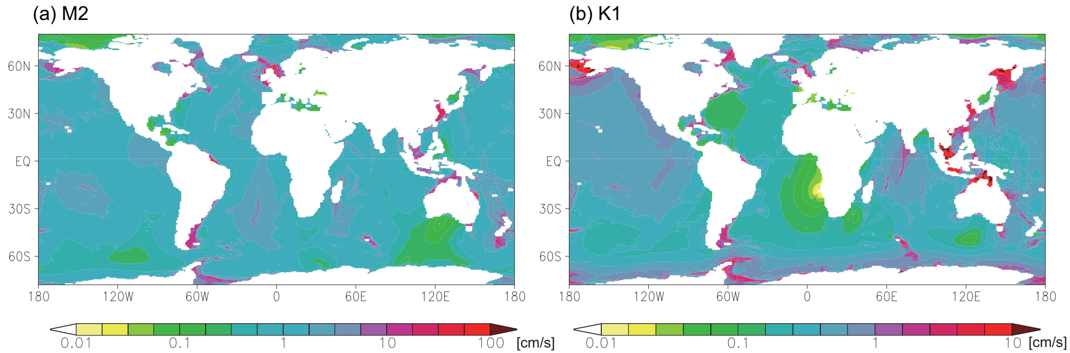

Fig. 6. Mean speed of the barotropic tidal currents $\overline{|u_{\mathrm{lt}}|}^{t}$ of **(a)** M2 tide and **(b)** K1 tide. The color shades are same as Fig. 1 of Müller et al. (2010), and the unit is cm s^{-1}.

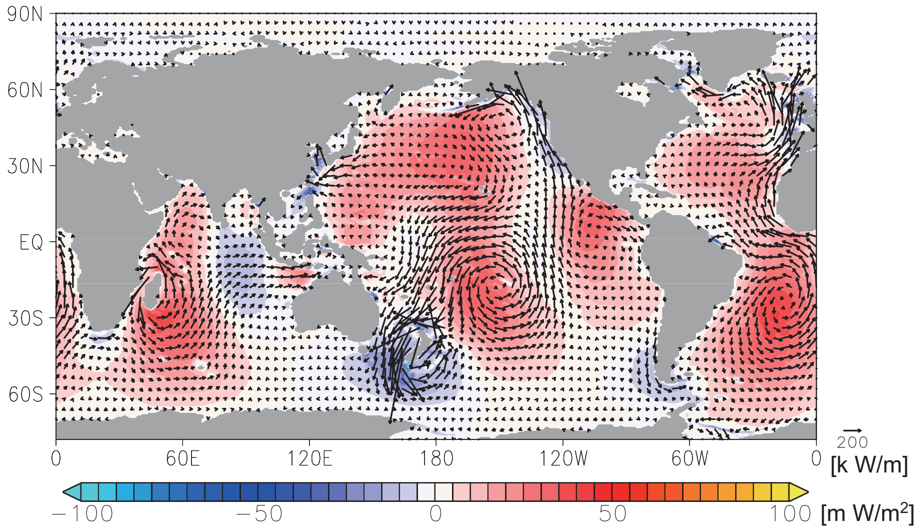

Fig. 7. Tidal energy flux *P* (vector) and power on the ocean *W* (color shades) in case M2. The unit length of the vectors is same as Fig. 1 of Egbert and Ray (2001).

OSD
10, 473–517, 2013

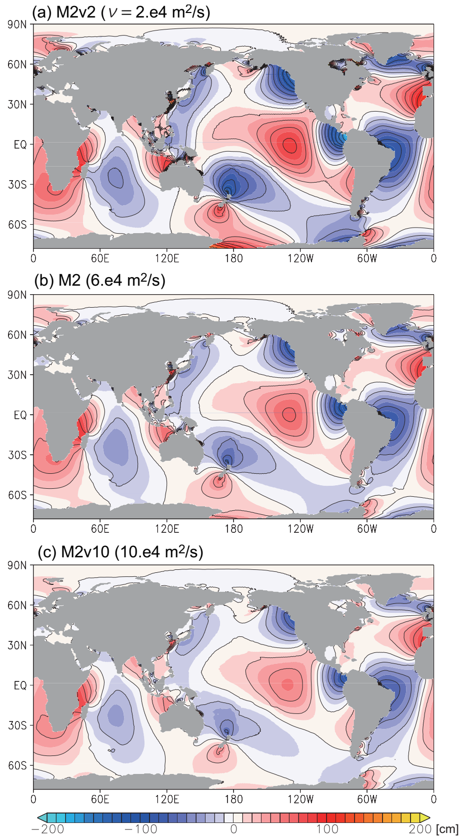

Fig. 8. Tidal height η_t at the end of the experiments (0:00 on 21 May 2001) in cases **(a)** M2v2 ($\nu = 2 \times 10^4\ \mathrm{m^2\,s^{-1}}$), **(b)** M2 ($6 \times 10^4$) and **(c)** M2v10 ($10 \times 10^4$). The contour interval is 20 cm.

OSD
10, 473–517, 2013

A practical scheme to introduce explicit tidal forcing into OGCM

K. Sakamoto et al.

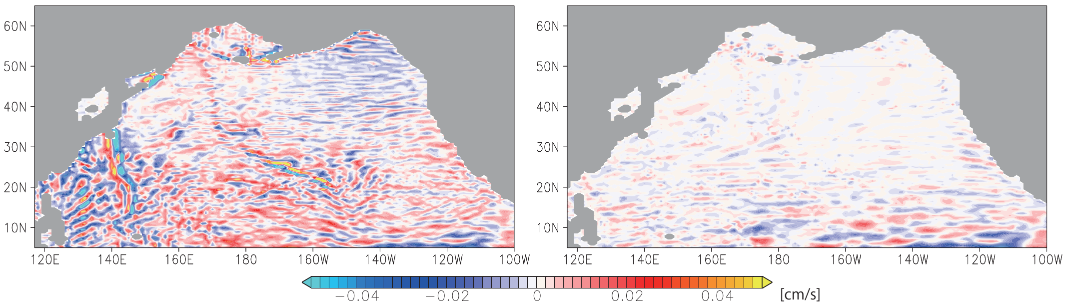

Fig. 9. Vertical velocity *w* at 1900 m depth in the North Pacific in **(a)** TIDE and **(b)** NOTIDE. The instantaneous distributions at the end of the experiment are shown.

OSD
10, 473–517, 2013

A practical scheme to introduce explicit tidal forcing into OGCM

K. Sakamoto et al.

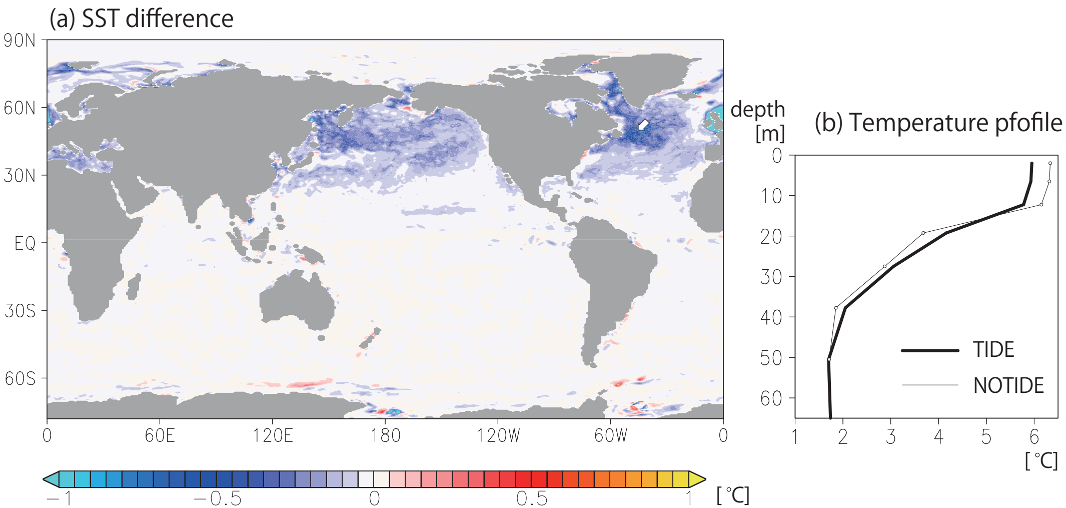

Fig. 10. (a) SST difference between TIDE and NOTIDE $\Delta\overline{T}^t$. **(b)** Vertical profiles of temperature $\overline{T}^t$ at the site (50° W, 50° N) (marked in **(a)**) in TIDE (thick line) and NOTIDE (thin). The vertical range from surface to 65 m depth is shown. Both of **(a)** and **(b)** use 25-h averages of the end of the experiments.

OSD
10, 473–517, 2013